Applied Catalysis B: Environmental 144 (2014) 379–385

Contents lists available at ScienceDirect

Applied Catalysis B: Environmental

journal homepage: www.elsevier.com/locate/apcatb

A study on upconversion UV–vis–NIR responsive photocatalytic activity and mechanisms of hexagonal phase $NaYF_4$:Yb^{3+},Tm^{3+}@TiO_2 core–shell structured photocatalyst

Wei Wang, Mingye Ding, Chunhua Lu*, Yaru Ni, Zhongzi Xu*

State Key Laboratory of Materials-Orient Chemical Engineering, College of Materials Science and Engineering, Nanjing University of Technology, Nanjing 210009, PR China

ARTICLE INFO

Article history:
Received 27 March 2013
Received in revised form 7 July 2013
Accepted 15 July 2013
Available online 24 July 2013

Keywords:
Photocatalysis
TiO_2
Near-infrared
Upconversion
Core–shell

ABSTRACT

A new core–shell structured composite consisting of upconversion hexagonal phase $NaYF_4$:Yb^{3+},Tm^{3+} (simply named $NaYF_4$) microrods and UV–vis–NIR driven anatase TiO_2 nanosheets with exposed high-reactive {0 0 1} facets has been prepared and shown to be an advanced NIR and sunlight activated photocatalyst. To understand the nature of NIR-driven photocatalysis of $NaYF_4$@TiO_2, various analysis methods are conducted. Structure analysis proved that TiO_2 is closely attached on the surface of $NaYF_4$ and can absorb all the converted NIR light (980 nm laser) for photocatalysis. As a result, the new photocatalyst gives higher photocatalytic activity in decomposing phenol and Rhodamine B (RhB) than their physical mixture and pure TiO_2 under the NIR and simulated sunlight irradiation. High-reactive hydroxyl radicals (•OH) analysis confirmed the superiority of the core–shell structure and the significant role of the upconversion material in using the NIR light to improve the photocatalytic activity of as-prepared TiO_2. Finally, a mechanism for NIR driven photocatalysis is proposed which will help to improve the structure design and functionality of new type of photocatalysts.

1. Introduction

In recently years, environment contamination, such as water and air pollution, has become a very serious problem all over the world. Photocatalysis is known as a very promising method in solving the problems for it is an environmentally friendly technique [1–3]. TiO_2, as one of the most investigated semiconductor photocatalysts, has been widely studied owing to its low cost, high efficiency, non-toxicity, and environment stability since 1972 [4–6]. However, the wide band gap of TiO_2 restricts its application significantly for it can only be activated by the UV light which only occupies ca. 5% of the solar energy. The visible (Vis) light and near-infrared (NIR) light which possess ca. 48% and ca. 45%, respectively, of the solar energy cannot be used for photocatalysis [7,8]. Therefore, making sufficient use of the photons with lower energy than the bandgap energy is very essential for the large scale application of TiO_2 to solve environment problems in the future.

To date, much effort has been devoted to enhance the light absorption ability of TiO_2 by extending its absorption region to the Vis and even NIR range. Several strategies, such as anionic and cationic doping, noble metals deposition, graphene/carbon nanotubes modification, and coupling with other semiconductors, have been used to reach this goal [9–14]. It is true that the absorption range of TiO_2 can be adjusted to the Vis and even NIR region with the help of these methods. However, some problems still existed for the introduced materials may increase the photogenerated electron–hole pair recombination in certain degree [15]. On the other hand, the photocatalytic activity of TiO_2 is also affected by the intensity of the irradiated light. Generally, the stronger intensity of the irradiated light, the higher photocatalytic efficiency will be acquired. Based on the already achieved results, converting the lower energy photons to higher energetic ones which can be absorbed by TiO_2 is an effective way to further enhance the photocatalytic activity [16–20].

With the development of materials science, upconversion materials, such as rare earth doped YF_3 and $NaYF_4$, have been discovered and studied widely [21–23]. Compared to YF_3, rare earth doped $NaYF_4$ is a more effective upconversion material which can emit bright light, such as green, blue, etc., under NIR light excitation. It is reasonable that the emitted bright fluorescence by rare earth doped $NaYF_4$ can be absorbed by TiO_2 for efficient photocatalysis reactions. Ren et al. prepared a composite composed of P25, YF_3:Yb^{3+},Tm^{3+}, and graphene for waste water purification [18]. However, the upconversion ability of YF_3:Yb^{3+},Tm^{3+} is low and P25 can only absorb the UV light. Xu et al. reported the preparation of N-TiO_2/$NaYF_4$:Yb^{3+},Tm^{3+} nanocomposite for near

* Corresponding authors. Tel.: +86 25 83587220; fax: +86 25 83587252.
E-mail addresses: lchnjut@163.com (C. Lu), xzznjut@163.com (Z. Xu).

0926-3373/$ – see front matter © 2013 Elsevier B.V. All rights reserved.
http://dx.doi.org/10.1016/j.apcatb.2013.07.035

infrared-triggered drug release [19]. Tang et al. reported the preparation of $NaYF_4$:Yb^{3+},Tm^{3+}@TiO_2 nanoparticles for methyl blue degradation [8]. However, the $NaYF_4$:Yb^{3+},Tm^{3+} reported is nanosized with the cubic phase which has relatively low upconversion ability compared to microsized hexagonal phase $NaYF_4$. On the other hand, the TiO_2 and $NaYF_4$ are physically mixed together which cannot transfer the upconverted light to TiO_2 sufficiently. More importantly, the reported TiO_2 is dominated by the low-reactive {1 0 1} facets and can only absorb the converted light before 500 nm.

In this work, for the first time, we reported the synthesis of core–shell structured photocatalysts composed of microsized hexagonal phase $NaYF_4$:Yb^{3+},Tm^{3+} and UV–vis–NIR driven TiO_2 nanosheets dominated by the high-reactive {0 0 1} facets. As is well known, the {0 0 1} facets of anatase TiO_2 is more reactive than the more thermodynamic stable {1 0 1} facets. More importantly, the microsized hexagonal phase $NaYF_4$:Yb^{3+},Tm^{3+} can convert NIR light efficiently to high-energetic UV and blue light which can be totally absorbed by the UV–vis–NIR driven TiO_2 nanosheets. A series of control experiments in the degradation of RhB and phenol under the 980 nm laser and simulated sunlight irradiation proves the superiority of the $NaYF_4$@TiO_2 core–shell structure than their physical mixture and pure TiO_2. The detection of high reactive •OH revealed the actual origin of the photocatalytic reaction by the NIR light.

2. Experimental

2.1. Preparation of TiO_2 nanosheets with exposed {0 0 1} facets

The UV–vis–NIR driven TiO_2 nanosheets dominated by the {0 0 1} facets were prepared according to the methods reported by our groups before [24]. Typically, 25 ml $Ti(OC_4H_9)_4$ was added slowly to 15 ml HF aqueous solution with a volume fraction of ca. 16% under continuous stirring at room temperature. The resulted suspension was transferred to a dry Teflon-lined autoclave with a capacity of 60 ml and treated at 240 °C for 24 h. The resulted blue product was washed and collected by centrifugation. Finally, the sample was dried in a vacuum oven at 80 °C overnight.

2.2. Preparation of hexagonal phase $NaYF_4$:Yb^{3+},Tm^{3+} microrods

The hexagonal phase $NaYF_4$:Yb^{3+},Tm^{3+} microrods were prepared according the methods reported before [25]. In a typical synthesis process, $Y(NO_3)_3$, NaF, $NaNO_3$, KNO_3 with a molar ratio of 1:4:64:32 were thoroughly mixed with an appropriate amount of ethanol in an agent mort. Then a small amount of $Tm(NO_3)_3$ and $Yb(NO_3)_3$ was added (the molar ratio of Y:Yb:Tm was 79.5:20:0.5). The mixture was grounded for 15 min and transferred into an alumina crucible (20 cm^3) heated at 400 °C for 2 h. After cooled down to room temperature, the as-prepared product, simply named $NaYF_4$, was washed with deionized water and dried in a vacuum oven at 80 °C overnight.

2.3. Preparation of $NaYF_4$@TiO_2 core–shell photocatalyst and physical mixture

0.05 g of TiO_2 nanosheets were added into 20 ml deionized water containing 0.2 ml thioglycolic acid. The resulted suspension was stirred for 3 h and then washed to obtain the thioglycolic acid functionalized TiO_2. Pure $NaYF_4$ microrods were dispersed in 20 ml deionized water containing 0.4 ml mercaptoethanol. After continuous stirring for 3 h, the product was washed to obtain the mercaptoethanol functionalized $NaYF_4$ microrods. The modified TiO_2 and $NaYF_4$ were mixed in 20 ml deionized water, and then heated at 160 °C for 3 h. Then the product was washed and collected to get the $NaYF_4$@TiO_2 core–shell structured photocatalyst. For comparison, pure $NaYF_4$ and TiO_2 were mixed together in deionized water by sonication and magnetic stirring, and then treated at 160 °C for 3 h. The resulted mixture is named $NaYF_4$/TiO_2(mix).

2.4. Characterization

Powder X-ray diffraction (XRD) measurements of as-prepared samples were conducted on an ARL X'TRA X-ray diffractometer using Cu K_α radiation (λ = 0.15406 nm) at a scanning rate of 5°/min. Filed emission scanning electron microscopy (FESEM) was performed with a S-4800 scanning electron analyzer with an accelerating voltage of 15 kV. UV–vis diffuse reflectance spectrum was performed with a 3101 spectrophotometer with $BaSO_4$ as the reflectance sample. Photoluminescence (PL) emission spectra were recorded on an FL3-221 fluorescence spectrophotometer equipped with a 450 W xenon lamp as the excitation source at room temperature. The surface chemical environments were analyzed by X-ray photoelectron spectra (XPS) on a PHI5000 VersaProbe system with monochromatic Al K_α X-rays. TEM analysis was conducted on a JEM-2010 electron microscope at an accelerating voltage of 200 kV. Electron paramagnetic resonance (EPR) spectra were recorded at 77 K on an EMX 10/12 spectrometer working in the X-band with 100 mg of the sample introduced into an EPR quartz probe cell. A 69920 type ARC Lamp Power Supply system and a commercial 980 nm NIR laser are used as the light source for photocatalysis.

2.5. Photocatalytic activity experiments and detection of photogenerated •OH

The photocatalytic activities of as-prepared samples under the 980 nm laser irradiation were measured by the degradation of RhB and phenol aqueous solution, respectively [17]. Typically, 20 mg of photocatalyst was suspended in 10 ml RhB or phenol aqueous solution (10^{-5} M) by sonication. Prior to irradiation, the suspension was stirred in the dark for 1 h to establish the adsorption–desorption equilibrium. Then the suspension was irradiated with the 980 nm laser with a current of 0.5 A for 1 h. 2 ml of the suspension was collected and then centrifuged to analyze the transparent aqueous solution with the spectrometer every 15 min. Photocatalytic activity measurements of the prepared photocatalysts under simulated sunlight irradiation were performed similarly [26]. RhB or phenol aqueous solution (50 ml, 10^{-5} M) and 20 mg of each photocatalyst were injected into a culture dish (d = 10 cm), followed by magnetic stirring for 1 h in the dark to establish the adsorption–desorption equilibrium. Then the simulated sunlight was applied to the photocatalytic reaction. A 5 ml of the solution was taken at certain time intervals (1 h) during the measurement process to record the absorption spectra of RhB and phenol, respectively.

The produced •OH under the 980 nm laser irradiation was analyzed by the PL technique and terephthalic acid was used as the probe molecule [27]. 2-Hydroxyterephthalic acid, a highly fluorescent compound, could be formed when the produced •OH interacted with the terephthalic acid in the water solution. The applied analysis method was almost the same with the photocatalytic activity measurement except the 10 ml pollutant aqueous solution was replaced by the terephthalic acid water solution (1 mM) with a concentration of NaOH (4 mM). The PL emission spectra of 2-hydroxyterephthalic acid were recorded on the fluorescence spectrophotometer by detecting the emission light with wavelength of 425 nm.

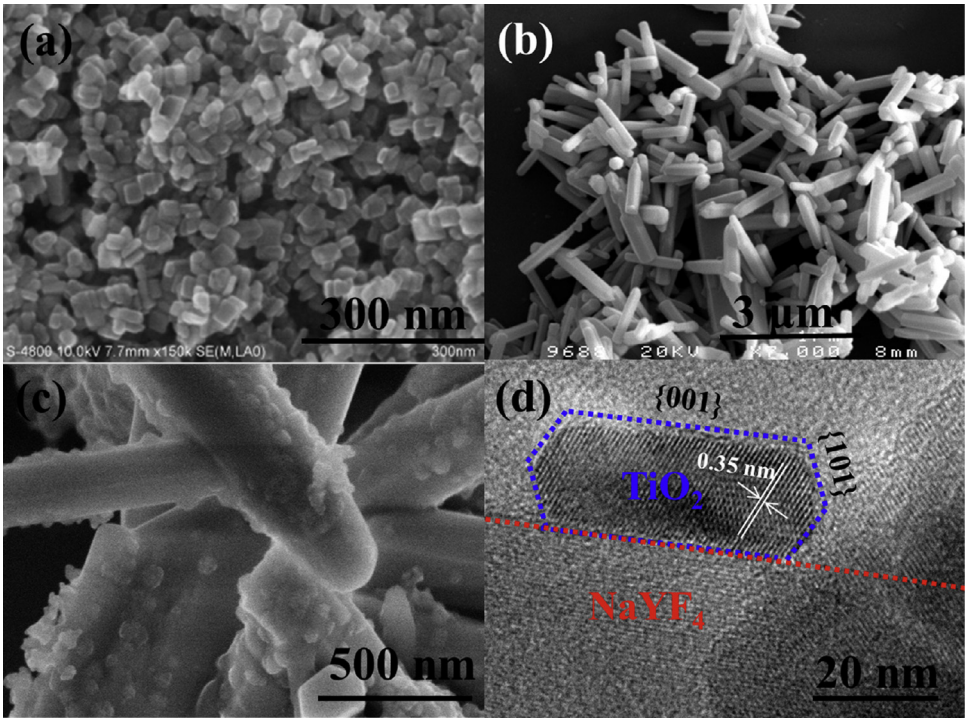

Fig. 1. Typical FESEM images of (a) UV–vis–NIR driven TiO_2 nanosheets with exposed {0 0 1} facets, (b) Yb^{3+}-Tm^{3+} doped hexagonal phase $NaYF_4$: microrods, and (c) $NaYF_4$@TiO_2 photocatalyst. (d) TEM image of $NaYF_4$@TiO_2 confirms the TiO_2 nanosheets dominated by the {0 0 1} facets and the close contact between TiO_2 and $NaYF_4$.

3. Results and discussion

3.1. Phase and morphological characterization

The morphology and size of as-synthesized materials were investigated by FESEM and TEM. Fig. 1a displays a typical FESEM image of pure TiO_2 nanosheets which preserve an average particle size of ca. 40 nm, and the outline of TiO_2 is sheet and square shaped. According to the symmetries of anatase TiO_2 and our previous studies, the two square facets can be ascribed to the {0 0 1} facets and the rest eight isosceles trapezoidal surfaces are the {1 0 1} facets [28–31]. The representative FESEM image of pure $NaYF_4$ microrods (Fig. 1b) shows that they are of a length roughly equal to 2 μm and diameter of ca. 300 nm. The surfaces of the microrods are very smooth. However, their surfaces become rather rough after loading the TiO_2 nanosheets (Fig. 1c). Obviously, the TiO_2 are uniformly assembled on the surface of the $NaYF_4$ microrods. The strong coupling between $NaYF_4$ and TiO_2 may due to the formation of chemical bonds between mercaptoethanol and thioglycolic acid, resulting in the formation of the core–shell structured $NaYF_4$@TiO_2. Fig. 1d gives a typical HRTEM image of $NaYF_4$@TiO_2 which shows the tight contact between the TiO_2 and $NaYF_4$. The TiO_2 nanosheet exhibits a *d*-spacing of 0.35 nm, corresponding to the (1 0 1) spacing of anatase TiO_2 [32,33]. Schematic illustration of the structure formation process is shown in Fig. 2. To find out whether TiO_2 could be coupled to $NaYF_4$ by physical adsorption, controlled experiments were conducted in the absence of surface modifiers. As shown in Fig. S1, TiO_2 does not adsorb well on $NaYF_4$ but agglomerated seriously with the method of simple physical mix.

Supplementary data associated with this article can be found, in the online version, at http://dx.doi.org/10.1016/j.apcatb.2013.07.035.

The XRD patterns of as-synthesized upconversion $NaYF_4$ and $NaYF_4$@TiO_2 are shown in Fig. 3. The position of all diffraction peaks (spectrum a) can be indexed to pure hexagonal phase $NaYF_4$ (JCPDS No. 28-1192). After TiO_2 was introduced to the $NaYF_4$ surface, several characteristic diffraction peaks of TiO_2 can be observed, corresponding to the anatase phase according to the JCPDS file No. 21-1272 (spectrum b). This result is in good agreement with the FESEM and TEM analysis and further confirms the exposure of the high-reactive {0 0 1} facets. With the load of TiO_2, $NaYF_4$ still maintains the hexagonal phase, indicating no phase change happened during the hydrothermal process.

3.2. Crystal inner structure and optical spectra investigation

In order to make sufficient use of the solar light for photocatalytic application, spectral match between the TiO_2 photocatalyst and the $NaYF_4$ upconversion material is very important. In essence, the light absorption ability of TiO_2 is closely related to its inner structure [7], XPS and EPR analysis were conducted to give a deep insight on this key point. As shown in Fig. 4a, the binding energy of Ti $2p_{3/2}$ fitted at 458.6 eV is the typical signal of Ti^{4+}. More importantly, a detectable shoulder with a binding energy of 458.1 eV which is the typical signal of Ti^{3+} appears in the spectrum [34–36].

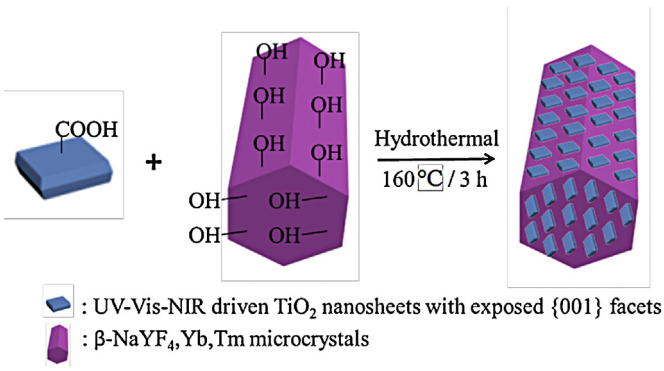

Fig. 2. Schematic illustration of preparation method and structure of $NaYF_4$@TiO_2 photocatalyst.

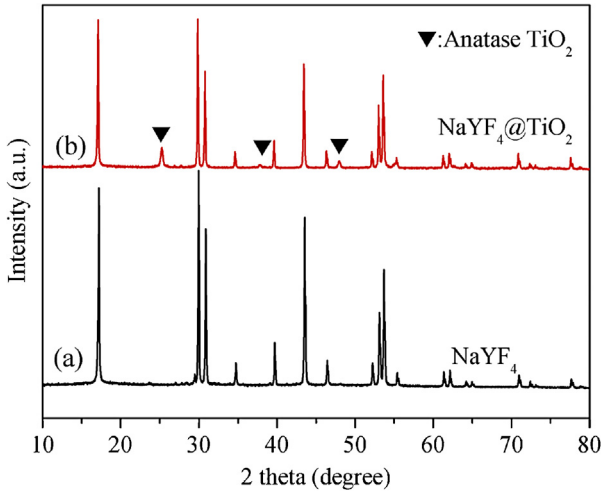

Fig. 3. XRD patterns of (a) as-prepared Yb^{3+}-Tm^{3+} doped hexagonal phase $NaYF_4$ and (b) core–shell structured $NaYF_4$@TiO_2 photocatalyst.

This result is also associated with the binding energy of F 1s (Fig. 4b). One of the F 1s peaks centered at 684 eV is to be associated with the surface F, which is resulted from the HF in controlling the formation of the {0 0 1} facets. The other one fitted at 684.9 eV can be ascribed to the bulk substitutional F, such as Ti–F–Ti. The decrease of F atoms on the TiO_2 surface will also introduce more OH groups [37]. This is in good agreement with our previous work which will favor the visible-light photocatalysis [9,24]. In Fig. 4c, the EPR signal with typical g values of $g_{\perp} = 1.992$ and $g_{||} = 1.962$ further confirms the existence of Ti^{3+} [37]. As a result of the unique inner structure, an intensity absorption band beyond 400 nm appears in as-prepared UV–vis–NIR driven TiO_2 nanosheets, comparing to the reference anatase TiO_2 which only absorb the UV light (Fig. 4d).

$NaYF_4$:Yb^{3+},Tm^{3+} is a typical upconversion luminescence material and the hexagonal phase is more efficient than the cubic phase [21,25]. Actually, upconversion is a multiphoton process in which the NIR excitation light, such as 980 nm, is converted to higher energy light via successive energy transfer processes [8]. Under the excitation of the 980 nm light, Yb^{3+} and Tm^{3+} doped $NaYF_4$ will emit high energy blue light (Fig. 5a, inset) with emission peaks centered at 354 nm, 469 nm, 537 nm, 644 nm, and 690 nm (Fig. 5a). The enlarged emission peak at 354 nm is shown in Fig. 5b. It is worth indicating that all the converted light of $NaYF_4$ is in the absorption spectrum range of TiO_2, which can be confirmed by the light absorption analysis shown in Fig. 4d.

After covering $NaYF_4$ microrods with TiO_2 nanosheets, obvious spectral differences can be observed, indicating efficient energy transfer (Fig. 5a). The emission intensity of the peak at 354 nm in the UV region decreases significantly and the peaks centered at 469 nm, 537 nm, 644 nm and 690 nm also decrease in certain degree in comparison with the pristine conversion spectrum of $NaYF_4$, indicating that the spectral change should be relevant to the introduced TiO_2 nanosheets [8,19]. The calculated light intensity ratios of the emission peak at 354 nm, 469 nm, 537 nm, 644 nm, and 690 nm of pure $NaYF_4$ and $NaYF_4$@TiO_2 are 13.24, 2.34, 5.98, 3.27, and 2.73, respectively. As is known, the surrounded TiO_2 may block the irradiated light to some extent, resulting in the reduction of the emission light intensity. However, the more of the short wavelength light was absorbed than the long wavelength light, suggesting that some of the converted light is absorbed by as-prepared TiO_2 [8,23]. This phenomenon can be ascribed to the intrinsic property of TiO_2 in absorbing more UV light than the visible and NIR light as confirmed by the previous light absorption analysis. When $NaYF_4$ and TiO_2 are physically mixed together, the emission intensity of the peaks is higher than that of $NaYF_4$@TiO_2, indicating that TiO_2 introduced by chemical modification can absorb the converted light more efficiently which is very beneficial for photocatalysis.

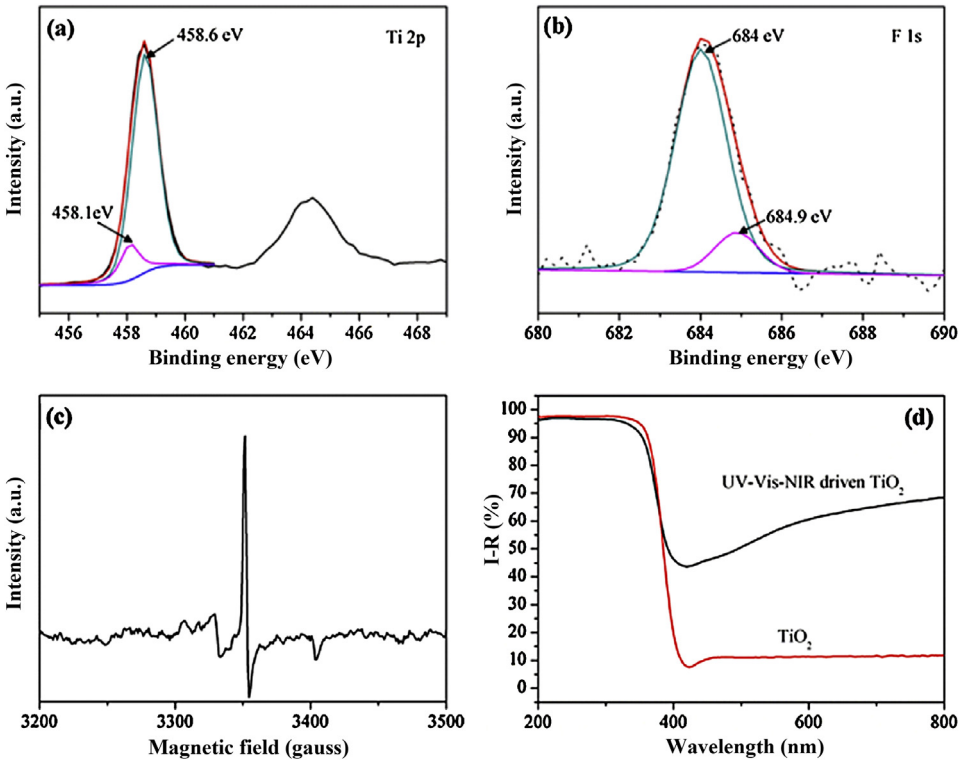

Fig. 4. High resolution (a) Ti 2p and (b) F 1s XPS spectra, and (c) Ti^{3+} EPR spectrum of UV–vis–NIR driven TiO_2 nanosheets with exposed {0 0 1} facets; (d) Light absorption spectra of as-prepared TiO_2 and reference anatase TiO_2.

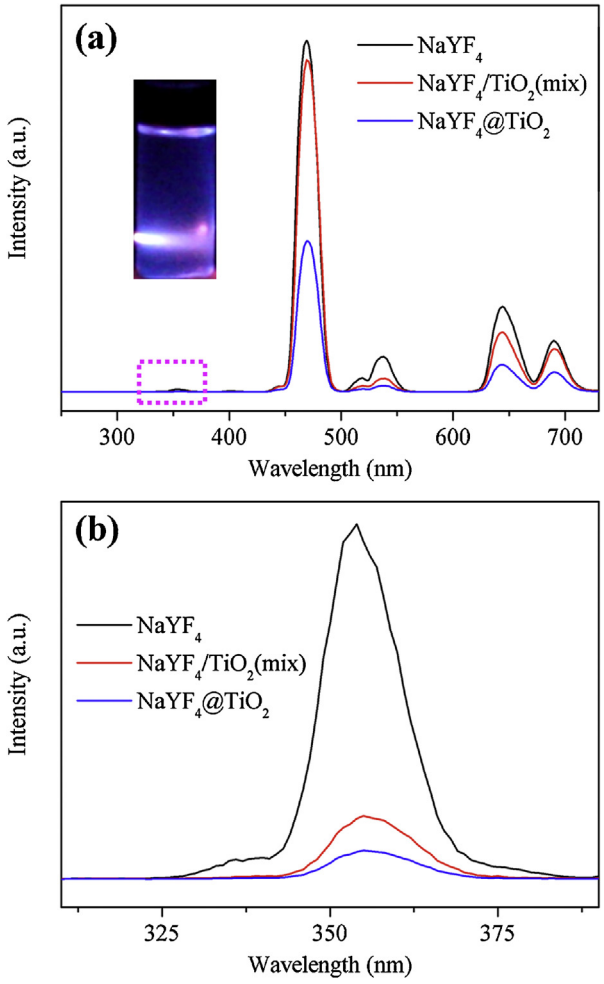

Fig. 5. (a) PL spectra of Yb^{3+}-Tm^{3+} doped $NaYF_4$, $NaYF_4$@TiO_2, and $NaYF_4$/TiO_2(mix) and (b) enlarged emission light centered at 354 nm under 980 nm laser excitation at room temperature.

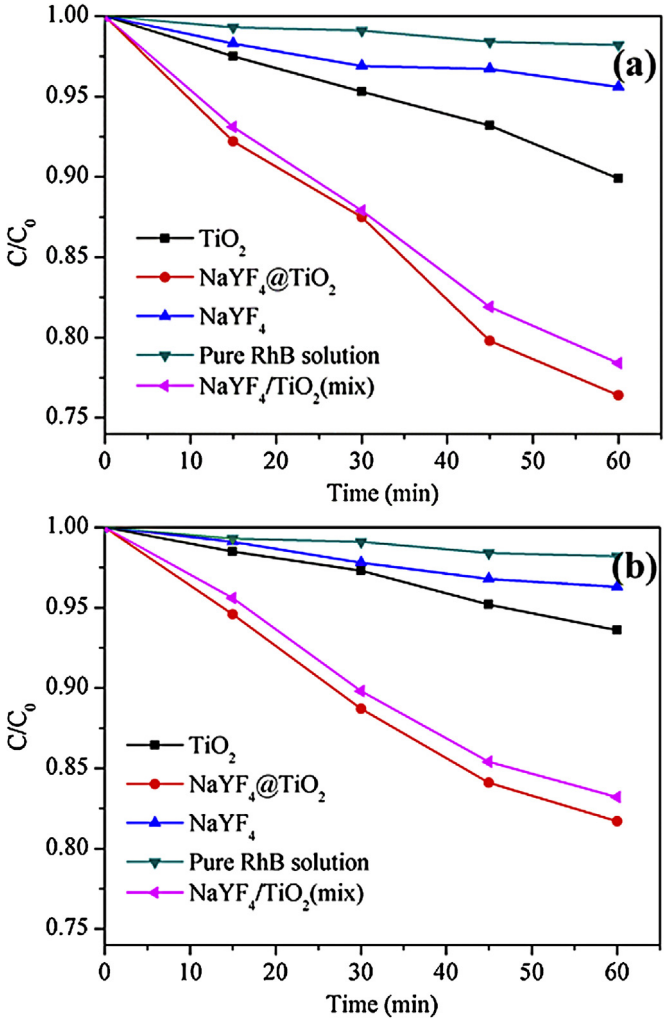

Fig. 6. (a) RhB and (b) phenol photodegradation efficiency with the presence of as-prepared samples under the 980 nm laser irradiation.

3.3. Photocatalytic activity and mechanisms study

RhB and phenol were used as the model pollutants to investigate the photocatalytic activity of as-prepared samples under the 980 nm laser and simulated sunlight irradiation. For the 980 nm laser irradiation, a 20 mg of the sample was dispersed into a glass bottle containing 10 ml of pollutant aqueous solution. To obtain the real photoactivity of $NaYF_4$@TiO_2, the reactions in the presence of single TiO_2, $NaYF_4$, $NaYF_4$/TiO_2(mix) and without any particles were also conducted. Fig. 6a shows the degradation efficiency curve of RhB under the 980 nm laser irradiation as a function of the irradiation time. Pure TiO_2 gives a slightly ability in decomposing the RhB which further confirms that it is responded to the NIR light, as clarified previously. Clearly, $NaYF_4$@TiO_2 gives the highest photocatalytic efficiency in the degradation of RhB which is also similar to the physical mixture of $NaYF_4$ and TiO_2, indicating that the uniform dispersion and close attachment of TiO_2 on the surface of $NaYF_4$ is very essential for TiO_2 to absorb the converted NIR light for photocatalytic reactions. In contrast, there are no direct contact interfaces between $NaYF_4$ and TiO_2 particles in their physical mixture, resulting in the random absorbance of light by TiO_2 [8]. On the other hand, both the higher reactivity of $NaYF_4$@TiO_2 and $NaYF_4$/TiO_2(mix) than pure TiO_2 proves the significant role of upconversion materials in converting the NIR photons to high energy photons for photocatalysis. As is known, the 980 nm laser irradiation will generate thermal energy which may influence the decomposition of RhB. However, only a little of the RhB was decomposed in the blank test implies that the thermal energy introduced here can be ignored. As reported before, organic dyes may mislead the photocatalytic activity of as-prepared photocatalysts [39,40]. To further confirm the real photocatalytic activity, phenol degradation was also investigated instead of RhB [9,41]. As can be seen from Fig. 6b, the degradation efficiency of phenol of RhB is different from that of RhB, however, the same degradation order was observed. This result indicates that the as-prepared core–shell structured upconversion photocatalysts can be used efficiently to solve the environment contamination resulted from the organic pollutants.

The generation of the high-reactive •OH which is often considered responsible for the degradation of organic molecules because of their strong oxidation ability was tested in order to verify the truly photocatalytic ability of $NaYF_4$@TiO_2 particles under the 980 nm laser irradiation [38]. Fig. 7a shows photoluminescence spectra of the terephthalic acid solution containing $NaYF_4$@TiO_2. At the beginning, almost no photoluminescence spectra of 2-hydroxyterephthalic acid were detected. After the irradiation of 980 nm laser, the spectra intensity increases with the increment of time, indicating that •OH has been produced during the photocatalytic reactions and the $NaYF_4$ can convert the NIR light for TiO_2 absorption efficiently. This result also implies that the degradation of RhB and phenol is originated from the excitation of TiO_2. The comparison of the fluorescence intensity of TiO_2, $NaYF_4$@TiO_2,

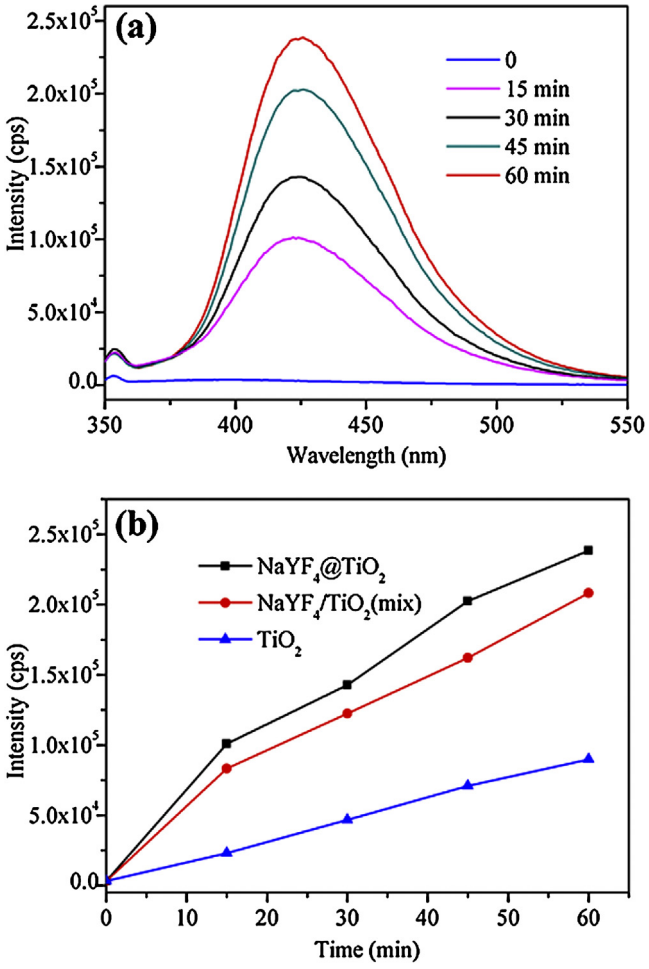

Fig. 7. (a) Time-dependent fluorescence spectra of terephthalic acid with the presence of $NaYF_4$@TiO_2 photocatalyst under the 980 nm laser irradiation; (b) comparison of the aqueous fluorescence intensity with the presence of $NaYF_4$@TiO_2, $NaYF_4$/TiO_2(mix) and TiO_2.

and $NaYF_4$/TiO_2(mix) under the NIR light irradiation in 60 min is shown in Fig. 7b. $NaYF_4$@TiO_2 produced more •OH radicals than $NaYF_4$/TiO_2(mix) and TiO_2, indicating $NaYF_4$@TiO_2 has the highest efficiency to absorb the converted light for photocatalysis. This result further confirms the efficient energy transfer in the core–shell structured photocatalyst between $NaYF_4$ and TiO_2.

Fig. 8 illustrates the diagram of upconversion luminescence processes of Yb^{3+}-Tm^{3+} doped hexagonal phase $NaYF_4$ upon the 980 nm light excitation. The absorption of pump photons only populates the $^2F_{5/2}$ level of Yb^{3+}, and then three successive energy transfers from Yb^{3+} to Tm^{3+} populate the $^3H_5$, $^3F_2$, and $^1G_4$ levels of Tm^{3+}. During the process, the $^3H_5$ and $^3F_2$ levels will relax nonradiatively to the $^3F_4$ and $^3H_4$ levels, respectively. And then the cross-relaxation between Tm^{3+} ions will result in populating the $^1D_2$ level, which may be promoted to the $^3P_2$ state via anther energy transfer from the excited Yb^{3+} and relaxes nonradiatively to the $^1I_6$ level [17]. After all these process, the excited Tm^{3+} ions will fall to lower energy levels: $^1D_2$–$^3H_6$ (354 nm), $^1G_4$–$^3H_6$ (469 nm), $^1D_2$–$^3H_5$ (537 nm), $^1G_4$–$^3F_4$ (644 nm) and $^3F_3$–$^3H_6$ (690 nm). As discussed earlier for the as-prepared anatase TiO_2 which is responsive to the UV–vis–NIR light, thus, the TiO_2 will be activated to produce holes and electrons in the valence band (VB) and conduction band (CB), respectively. The photogenerated electrons and pairs will migrate from the inner region to the surfaces of TiO_2, resulting in the formation of high reactive species, such as •OH, to take part

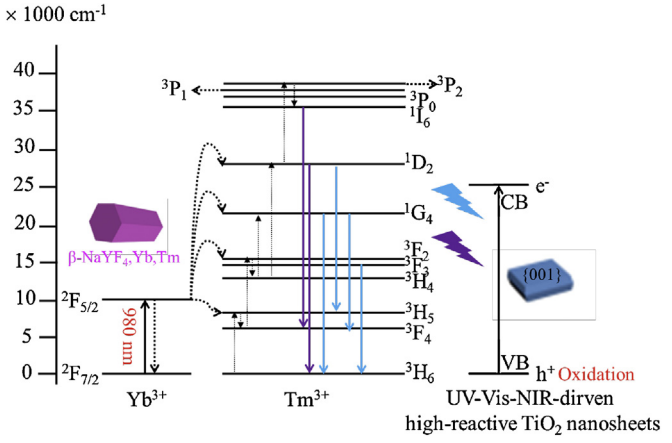

Fig. 8. Schematic illustration of energy transfer mechanism from Yb^{3+}-Tm^{3+} doped hexagonal phase $NaYF_4$ microrods to {0 0 1} facets dominated UV–vis–NIR driven TiO_2 nanosheets under the 980 nm light irradiation.

in the photocatalytic reactions. This is also benefited from the close attachment between TiO_2 and $NaYF_4$.

In order to investigate the practical application of the photocatalyst, simulated sunlight was also used as the light source. Fig. 9a shows that RhB concentration has little change when $NaYF_4$ was

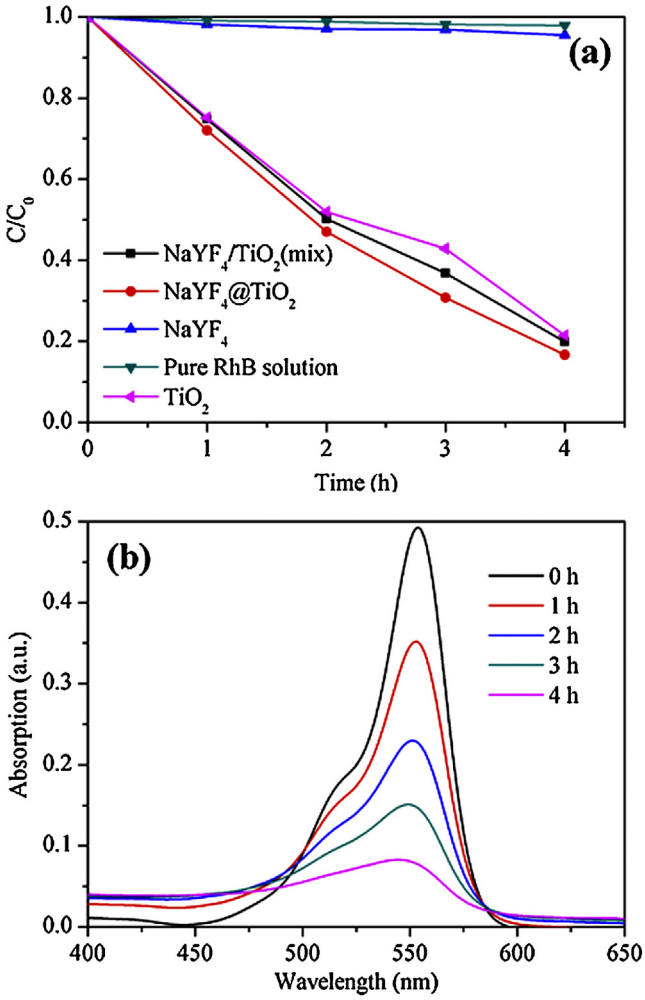

Fig. 9. (a) RhB photodegradation efficiency with the presence of as-prepared samples and (b) RhB absorbance spectra catalyzed by $NaYF_4$@TiO_2 under simulated sunlight irradiation.

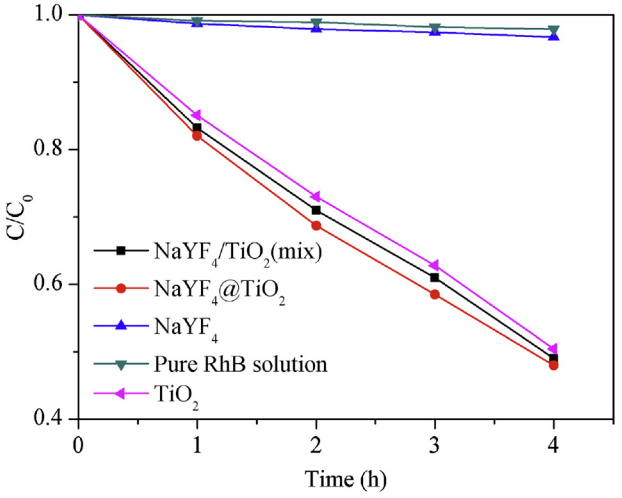

Fig. 10. Phenol photodegradation efficiency with the presence of as-prepared samples under the simulated sunlight irradiation.

suspended in the solution. After the introduction of photocatalysts, $NaYF_4$@TiO_2 also gives the highest efficiency, and this is the same with the result under the 980 nm laser irradiation. The corresponding absorption spectra of RhB are shown in Fig. 9b. Furthermore, the photocatalytic activities of TiO_2, $NaYF_4$@TiO_2 and $NaYF_4$/TiO_2(mix) are very close to each other. This may be due to that the converted NIR energy is much less than that of the UV and visible light for the TiO_2 we prepared can absorb most of the sunlight in the UV–vis–NIR range. Similar photocatalytic results are also observed for the phenol degradation (Fig. 10). These results indicate that make sufficient use of the sunlight for large scale applications of TiO_2 to solve environmental contaminants by employing the upconversion materials is a promising method.

4. Conclusions

Upconversion luminescence hexagonal phase $NaYF_4$:Yb^{3+},Tm^{3+} microrods were prepared and UV–vis–NIR responsive anatase TiO_2 nanosheets with exposed {0 0 1} facets were closely attached to the $NaYF_4$:Yb^{3+},Tm^{3+} surface to form a new core–shell structured photocatalyst by chemical modification. The degradation of RhB and phenol with $NaYF_4$@TiO_2 upon the 980 nm laser and simulated sunlight irradiation demonstrated the NIR-driven photocatalytic ability. Compared to the physical mixture of $NaYF_4$ and TiO_2, the closely attached core–shell structure revealed its superiority in making sufficient use the converted NIR light for photocatalysis. The detection of photogenerated •OH confirmed the superiority of the core–shell structure and the proposed mechanism of NIR-driven photocatalytic degradation of the pollutants. This work is anticipated to promote the practical applications of photocatalysts making sufficient use of sunlight to solve energy and environment contamination problems.

Supporting information

SEM image of the physical mixture of $NaYF_4$ and TiO_2 is shown in Fig. S1.

Acknowledgements

This work was supported by the National Natural Science Foundation of China (Grant No. 20901040/B0111), the Key University Science Research Project of Jiangsu Province (No. 10KJA430016), Innovation Foundation for Graduate Students of Jiangsu Province China (CXLX11_0346), and a project funded by the Priority Academic Program Development of Jiangsu Higher Education Institutions (PAPD).

References

[1] C. Chen, W. Ma, J. Zhao, Chemical Society Reviews 39 (2010) 4206–4219.
[2] T. Fröschl, U. Hörmann, P. Kubiak, G. Kučerová, M. Pfanzelt, C.K. Weiss, R.J. Behm, N. Hüsing, U. Kaiser, K. Landfester, M. Wohlfahrt-Mehrens, Chemical Society Reviews 41 (2012) 5313–5360.
[3] X. Chen, S. Shen, L. Guo, S.S. Mao, Chemical Reviews 110 (2010) 6503–6570.
[4] A. Fujishima, K. Honda, Nature 238 (1972) 37–38.
[5] D. Ulrike, Surface Science Reports 48 (2003) 53–229.
[6] A. Fujishima, X. Zhang, D. Tryk, Surface Science Reports 63 (2008) 515–582.
[7] X. Chen, L. Liu, P.Y. Yu, S.S. Mao, Science 331 (2011) 746–750.
[8] Y. Tang, W. Di, X. Zhai, R. Yang, W. Qin, ACS Catalysis 3 (2013) 405–412.
[9] W. Wang, C. Lu, Y. Ni, M. Su, Z. Xu, Applied Catalysis B: Environmental 127 (2012) 28–35.
[10] W. Wang, C. Lu, Y. Ni, M. Su, W. Huang, Z. Xu, Applied Surface Science 258 (2012) 8696–8703.
[11] W.-J. An, W.-N. Wang, B. Ramalingam, S. Mukherjee, B. Daubayev, S. Gangopadhyay, P. Biswas, Langmuir 28 (2012) 7528–7534.
[12] J.S. Lee, K.H. You, C.B. Park, Advanced Materials 24 (2012) 1084–1088.
[13] J. Yu, T. Ma, S. Liu, Physical Chemistry Chemical Physics 13 (2011) 3491–3501.
[14] H. Zhu, B. Yang, J. Xu, Z. Fu, M. Wen, T. Guo, S. Fu, J. Zuo, S. Zhang, Applied Catalysis B: Environmental 90 (2009) 463–469.
[15] M. D'Arienzo, N. Siedl, A. Sternig, R. Scotti, F. Morazzoni, J. Bernardi, O. Diwald, The Journal of Physical Chemistry C 114 (2010) 18067–18072.
[16] D.W. Manley, R.T. McBurney, P. Miller, R.F. Howe, S. Rhydderch, J.C. Walton, Journal of the American Chemical Society 134 (2012) 13580–13583.
[17] C. Li, F. Wang, J. Zhu, J.C. Yu, Applied Catalysis B: Environmental 100 (2010) 433–439.
[18] L. Ren, X. Qi, Y. Liu, Z. Huang, X. Wei, J. Li, L. Yang, J. Zhong, Journal of Materials Chemistry 22 (2012) 11765–11771.
[19] Q.C. Xu, Y. Zhang, M.J. Tan, Y. Liu, S. Yuan, C. Choong, N.S. Tan, T.T.Y. Tan, Advanced Healthcare Materials 1 (2012) 470–474.
[20] Z.-X. Li, F.-B. Shi, T. Zhang, H.-S. Wu, L.-D. Sun, C.-H. Yan, Chemical Communications 47 (2011) 8109–8111.
[21] W.J. Huang, C.H. Lu, C.F. Jiang, W. Wang, J.B. Song, Y.R. Ni, Z.Z. Xu, Journal of Colloid and Interface Science 376 (2012) 34–39.
[22] M.Y. Ding, W.J. Huang, L.H. Cao, C.H. Lu, J.B. Song, Y.R. Ni, Z.Z. Xu, Materials Letters 86 (2012) 58–61.
[23] Z. Li, C. Li, Y. Mei, L. Wang, G. Du, Y. Xiong, Nanoscale 5 (2013) 3030–3036.
[24] W. Wang, C.-H. Lu, Y.-R. Ni, J.-B. Song, M.-X. Su, Z.-Z. Xu, Catalysis Communications 22 (2012) 19–23.
[25] X. Zhang, P. Yang, C. Li, D. Wang, J. Xu, S. Gai, J. Lin, Chemical Communications 47 (2011) 12143–12145.
[26] W. Wang, C. Lu, Y. Ni, Z. Xu, Applied Catalysis B: Environmental 129 (2013) 606–613.
[27] Q. Xiang, J. Yu, M. Jaroniec, Physical Chemistry Chemical Physics 13 (2011) 4853–4861.
[28] W. Wang, C. Lu, Y. Ni, Z. Xu, CrystEngCommunity 15 (2013) 2537–2543.
[29] H.G. Yang, C.H. Sun, S.Z. Qiao, J. Zou, G. Liu, S.C. Smith, H.M. Cheng, G.Q. Lu, Nature 453 (2008) 638–641.
[30] C.Z. Wen, H.B. Jiang, S.Z. Qiao, H.G. Yang, G.Q. Lu, Journal of Materials Chemistry 21 (2011) 7052–7061.
[31] Y. Wang, H. Zhang, Y. Han, P. Liu, X. Yao, H. Zhao, Chemical Communications 47 (2011) 2829–2831.
[32] J. Shen, Y. Zhu, X. Yang, C. Li, Journal of Materials Chemistry 22 (2012) 13341–13347.
[33] M. Čaplovičová, P. Billik, Ľ. Čaplovič, V. Brezová, T. Turáni, G. Plesch, P. Fejdi, Applied Catalysis B: Environmental 117–118 (2012) 224–235.
[34] G. Wang, H. Wang, Y. Ling, Y. Tang, X. Yang, R.C. Fitzmorris, C. Wang, J.Z. Zhang, Y. Li, Nano Letters 11 (2011) 3026–3033.
[35] G. Liu, H.G. Yang, X. Wang, L. Cheng, H. Lu, L. Wang, G.Q. Lu, H.-M. Cheng, The Journal of Physical Chemistry C 113 (2009) 21784–21788.
[36] S. Hoang, S.P. Berglund, N.T. Hahn, A.J. Bard, C.B. Mullins, Journal of the American Chemical Society 134 (2012) 3659–3662.
[37] A.M. Czoska, S. Livraghi, M. Chiesa, E. Giamello, S. Agnoli, G. Granozzi, E. Finazzi, C.D. Valentin, G. Pacchioni, The Journal of Physical Chemistry C 112 (2008) 8951–8956.
[38] J. Zhang, J. Xi, Z. Ji, Journal of Materials Chemistry 22 (2012) 17700–17708.
[39] X.L. Yan, T. Ohno, K. Nishijima, R. Abe, B. Ohtani, Chemical Physics Letters 429 (2006) 606–610.
[40] B. Ohtani, Chemistry Letters 37 (2008) 216–229.
[41] R. Su, R. Tiruvalam, Q. He, et al., ACS Nano 6 (2012) 6284–6292.